Supplementary Material (ESI) for PCCP
This journal is © the Owner Societies 2009

Supplemental Material to Calculation of NMR parameters in ionic solids by an improved self-consistent embedded cluster method

Johannes Weber
Jörn Schmedt auf der Günne[†]
Department of Chemistry and Biochemistry, Ludwig-Maximilians-Universität, D-81377 Munich, Germany.

Contents

S1 Theoretical foundation of the cluster approach **3**

S2 Crystal structures and quantum clusters used in this work **8**
- S2.1 Crystal structure of $Mg_2P_4O_{12}$ 8
- S2.2 Crystal structure of α-$Mg_3(PO_4)_2$ 12
- S2.3 Crystal structure of α-$Mg_2P_2O_7$ 13
- S2.4 Crystal structure of MgP_4O_{11} 16

S3 Calculation details for the ^{31}P $\sigma \leftrightarrow \delta$ calibration curve **18**

S4 Full references to abbreviated citations **25**

[†] author to whom correspondence should be addressed, email: gunnej@cup.uni-muenchen.de

List of Figures

S1 Compensation effect of magnetic shielding contributions 4
S2 Nucleus independent chemical shift of rare gas atoms at various distances r from the nucleus. 7
S3 Crystal structure of the $Mg_2P_4O_{12}$ viewed along the b axis. 9
S4 Further $Mg_2P_4O_{12}$ clusters. (a): $[Mg_2P_4O_{12}]^0_7$, (b): $[Mg_2P_4O_{12}]^0_{13}$. P sites with off-centerd labels indicate reference points for the local expansion. 11
S5 Crystal structure of α-$Mg_3(PO_4)_2$ as reported in[1], 2x2x2 unit cells viewed along c axis. 12
S6 Unit cell of α-$Mg_2P_2O_7$ viewed along b axis. 16
S7 Unit cell of MgP_4O_{11} viewed along the a axis. 17
S8 Correlation between experimental chemical shifts and calculated magnetic shieldings. *top*: experimental structures were used, *bottom*: quantum chemically optimzed structures were used. 23

S1 Theoretical foundation of the cluster approach

The local character of NMR properties has frequently been the basis of approximations used in early calculations of NMR parameters[2–6]. As far as we know no thorough investigation has been conducted in order to justify the cluster approach or to give guidelines for the QC setup, however.

The magnetic shielding tensor is $\overleftrightarrow{\sigma}^N$ defined by

$$\mathbf{B}_{ind}(\mathbf{r}_N) = -\overleftrightarrow{\sigma}^N \cdot \mathbf{B}_{ext} \tag{S1}$$

where $\mathbf{B}_{ind}(\mathbf{r}_N)$ is the induced magnetic field at the position $\mathbf{r}_N$ of the nucleus and $\mathbf{B}_{ext}$ is the external magnetic field in which the sample is immersed. The spatial contributions to $\mathbf{B}_{ind}(\mathbf{r}_N)$ in SI based atomic units are given by the integrand in Biot-Savart's law[7,8]

$$\mathbf{B}_{ind}(\mathbf{r}_N) = \frac{1}{c^2}\int_V \frac{\mathbf{j}(\mathbf{r}') \times (\mathbf{r}_N - \mathbf{r}')}{|\mathbf{r}_N - \mathbf{r}'|^3} d^3r' \qquad , \tag{S2}$$

where $\mathbf{j}(\mathbf{r}')$ is the current density (for closed shell systems and ordinary magnetic field strengths $\mathbf{j}(\mathbf{r}')$ is sufficiently described by the first-order current density induced by $\mathbf{B}_{ext}$) and $(\mathbf{r}_N - \mathbf{r}') = \mathbf{r}$ is the difference vector between the position of the nucleus and a small volume element at position $\mathbf{r}'$. As the integrand scales formally with r^{-2}, the contributions from farther distant volume elements to $\mathbf{B}_{ind}(\mathbf{r}_N)$ decrease quadratically and according to eq. (S1) the same is true for $\overleftrightarrow{\sigma}^N$.[†] The role of $\mathbf{j}(\mathbf{r}')$ which depends on the specific molecular structure, has been neglected in this consideration. In most cases a compensating effect can be expected from different $\mathbf{j}(\mathbf{r}')$ contributions at farther distances, which leads to a total decay of spatial contributions to $\overleftrightarrow{\sigma}^N$ much faster than r^{-2}. This can be explained as follows: for a static $\mathbf{B}_{ext}$ one obtains $\nabla\mathbf{j} = 0$, i.e. the current density is represented by loops of closed isolines. Because the atomic structure is essentially maintained in a crystal, most loops enclose individual nuclei, only. In each loop that does not enclose $\mathbf{r}_N$, i.e. the nucleus of interest, the current density $\mathbf{j}(\mathbf{r}_{l1})$ in a small segment $l1$ has a counterpart of antiparallel current density $\mathbf{j}(\mathbf{r}_{l2})$ in a second segment $l2$ of that loop, which leads to a partial compensation of the shielding contributions at $\mathbf{r}_N$ resulting from $\mathbf{j}(\mathbf{r}_{l1})$ and $\mathbf{j}(\mathbf{r}_{l2})$. Figure S1 shows the compensation effect for a ringlike loop shape. Any other loop shape will display a compensation effect, too.

The expectation is supported by several calculations on the distance-dependence of $\overleftrightarrow{\sigma}^N$ in a pair of interacting atoms[9–12]. For two neutral atoms a decay of approximately r^{-6} has been found for the isotropic magnetic shielding σ^N in the long range limit (r is now the interatomic distance). In an atom-ion pair a decay of $\sim r^{-4}$ was found for σ^N. A decay of r^{-3} has been found for the shielding anisotropy $\sim\sigma^N_{aniso}$ for a pair of neutral atoms. Hence, the contributions to $\overleftrightarrow{\sigma}^N$ from far distant interactions can be neglected at some point without significant loss in accuracy and the cluster approach is justified.

[†] Considering contributions to $\mathbf{B}_{ind}(\mathbf{r}_N)$ from spherical shells $S = [\mathbf{r}', \mathbf{r}' + d\mathbf{r}']$ around N, no decay with increasing $\mathbf{r}'$ is obtained.

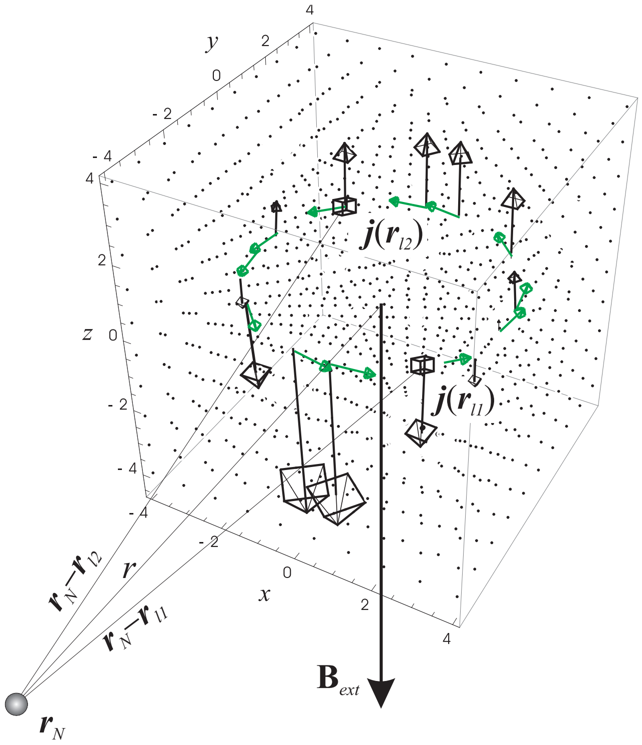

Figure S1: Compensation effect of magnetic shielding contributions. Assume an induced current density $\mathbf{j}(\mathbf{r}')$ (green arrows) on a ring at large distance r from the nuclear position $\mathbf{r}_N$. Contributions to $\mathbf{B}_{ind}(\mathbf{r}_N)$ from different small volume elements of the ring current are visualized by black arrows (located at the respective ring segments). The contributions from $\mathbf{r}_{l1}$ and $\mathbf{r}_{l2}$ compensate each other partly. The same holds for any other pair of opposite ring segments.

An advantage of the cluster approach is its flexibility. In a limited region the cluster can usually be described by more a complete basis and by a more accurate quantum chemical model as compared to the description in periodic calculations. Typically, a triple-ζ basis plus a double set of polarization functions and a model like hybride DFT that takes account of electron correlation and exact exchange should be considered as minimum requirement for reliable results. Farther distant contributions can be treated at increasing levels of approximation. We note that the local character of NMR properties is also used for approximations in periodic approaches[13,14], albeit its usage in the cluster modelling is more radical.

The electrostatic approximation

Although the electrostatic approximation is frequently used it has seldomly been defined precisely. This is done in the following in order to point out the different types of systematic deviations that emerge. Using the notation in atomic units the total non-relativistic electronic Hamiltonian of an extended system is given as

$$\begin{aligned}\hat{H} &= -\frac{1}{2}\sum_{i=1}^{n}\Delta_i - \sum_{i=1}^{n}\sum_{K=1}^{N}\frac{Z_K}{r_{iK}} + \sum_{i=1}^{n}\sum_{j>i}^{n}\frac{1}{r_{ij}} + \sum_{K=1}^{N}\sum_{L>K}^{N}\frac{Z_K Z_L}{R_{KL}} \\ &= \quad \hat{T}_e \quad + \quad \hat{V}_{Ne} \quad + \quad \hat{V}_{ee} \quad + \quad \hat{V}_{NN}\end{aligned} \tag{S3}$$

where indices i, j run over all electrons and indices K, L run over all nuclei. Solving the Schroedinger equation for $\hat{H}$ will give the full wave function $\Psi(\mathbf{x}_i, \mathbf{x}_K)$ of the system. When the total system is partitioned in a quantum cluster (QC) and an outer part (OP), the Hamiltonian can be reformulated in twelve different terms

$$\begin{aligned}\hat{H} = {} & \hat{T}_e^{QC} + \hat{V}_{Ne}^{QC} + \hat{V}_{ee}^{QC} + \hat{V}_{NN}^{QC} \\ + {} & \hat{T}_e^{OP} + \hat{V}_{Ne}^{OP} + \hat{V}_{ee}^{OP} + \hat{V}_{NN}^{OP} \\ - {} & \sum_{i\in QC}\sum_{K\in OP}\frac{Z_K}{r_{iK}} + \sum_{i\in QC}\sum_{j\in OP}\frac{1}{r_{ij}} + \sum_{K\in QC}\sum_{L\in OP}\frac{Z_K Z_L}{R_{KL}} - \sum_{i\in OP}\sum_{K\in QC}\frac{Z_K}{r_{iK}}\end{aligned} \tag{S4}$$

with $\hat{T}_e^{QC} = -\frac{1}{2}\sum_{i\in QC}\Delta_i$, $\hat{V}_{Ne}^{QC} = -\sum_{i\in QC}\sum_{K\in QC}\frac{Z_K}{r_{iK}}$, $\hat{V}_{ee}^{QC} = \sum_{i\in QC}\sum_{j\in QC>i}\frac{1}{r_{ij}}$, $\hat{V}_{NN}^{QC} = \sum_{K\in QC}\sum_{L\in QC>K}\frac{Z_K Z_L}{R_{KL}}$, $\hat{T}_e^{OP} = -\frac{1}{2}\sum_{i\in OP}\Delta_i$, $\hat{V}_{Ne}^{OP} = -\sum_{i\in OP}\sum_{K\in OP}\frac{Z_K}{r_{iK}}$, $\hat{V}_{ee}^{OP} = \sum_{i\in OP}\sum_{j\in OP>i}\frac{1}{r_{ij}}$, and $\hat{V}_{NN}^{OP} = \sum_{K\in OP}\sum_{L\in OP>K}\frac{Z_K Z_L}{R_{KL}}$. The first four terms of (S4) represent the Hamiltonian of the QC region and may be denoted as $\hat{H}_{QC}$

$$\hat{H}_{QC} = \hat{T}_e^{QC} + \hat{V}_{Ne}^{QC} + \hat{V}_{ee}^{QC} + \hat{V}_{NN}^{QC} \tag{S5}$$

Solving the Schroedinger equation for $\hat{H}_{QC}$ leads to the “undistorted” wave function $\Psi_{QC}(\mathbf{x}_{i\in QC}, \mathbf{x}_{K\in QC})$ of the non-embedded QC. Likewise, terms five to eight may be collected in a Hamiltonian named $\hat{H}_{OP}$ as they exclusively describe the outer part. Solving the Schroedinger equation for $\hat{H}_{OP}$ leads to the OP wave function $\Psi_{OP}(\mathbf{x}_{i\in OP}, \mathbf{x}_{K\in OP})$. The remaining terms in (S4) describe interactions between the QC and the OP.

In the embedded cluster approximation with point charges representing the OP $\hat{H}_{QC}$ remains unchanged. $\hat{H}_{OP}$ may be dropped as the electrons and nuclei in the outer part are replaced by effective atomic charges q_k. This adds only a constant energy to the system. The total Hamiltonian for the embedded QC then takes the form

$$\hat{H}_{eQC} = \hat{H}_{QC} - \sum_{i\in QC}\sum_{k\in OP}\frac{q_k}{r_{ik}} + \sum_{K\in QC}\sum_{k\in OP}\frac{Z_K q_k}{r_{Kk}} \tag{S6}$$

The second and third term in (S6) replace the exact QC-OP interaction terms nine to twelve in (S4). Solving the Schroedinger equation for $\hat{H}_{eQC}$ will result in an approximate wave function $\Psi_{eQC}(\mathbf{x}_{i\in QC}, \mathbf{x}_{K\in QC}, q_k(\mathbf{r}_k))$ which is similar to $\Psi_{QC}(\mathbf{x}_{i\in QC}, \mathbf{x}_{K\in QC})$, but distorted because of the presence of the embedding charges. In favorable cases the distortion of Ψ_{eQC} leads to a higher similarity with the exact WF $\Psi(\mathbf{x}_i, \mathbf{x}_K)$ in the QC region. The point charge approximation is a drastic simplification of the system as *(i)* the exchange symmetry between electrons in the QC and the OP is neglected, *(ii)* the charge distribution in the OP which creates an electrostatic potential in the QC region is approximated by a point charge array, *(iii)* the electronic wave function is restricted to the QC region.

In principle each quantum chemical observable or property depends on the full WF $\Psi(\mathbf{x}_i, \mathbf{x}_k)$. A property is termed as “local” if it can be derived without significant loss in accuracy from an approximate WF $\Psi_{eQC}(\mathbf{x}_{i\in QC}, \mathbf{x}_{k\in QC}, q_k(\mathbf{r}_k))$ and corresponding subspace operators. Now, we consider the nuclear magnetic shielding $\overleftrightarrow{\sigma}^N$ as a local property. In analogy to Ramsay’s sum-over-states expression for the exact WF[15] we obtain

$$
\begin{aligned}
\sigma^N_{eQC,uv} &= \sigma^{N,dia}_{eQC,uv} + \sigma^{N,para}_{eQC,uv} && \text{(S7)}\\
&= \frac{1}{2c^2}\left\langle \Psi_{eQC,0} \middle| \sum_i \frac{(\mathbf{r}_{iO}\mathbf{r}_{iN})\delta_{uv} - r_{iO,v}r_{iN,u}}{r^3_{iN}} \middle| \Psi_{eQC,0} \right\rangle \\
&+ \frac{1}{2c^2}\sum_{n\neq 0} \frac{\left\langle \Psi_{eQC,n} \middle| \sum_i \mathbf{l}_{iN,v} \middle| \Psi_{eQC,0} \right\rangle \left\langle \Psi_{eQC,0} \middle| \frac{\sum_i \mathbf{l}_{iN,u}}{r^3_{iN}} \middle| \Psi_{eQC,n} \right\rangle}{E_{eQC,0} - E_{eQC,n}} + c.c. && \text{(S8)}\\
\text{with} \quad & \mathbf{l}_{iO,v} = -\mathrm{i}\mathbf{r}_{iO} \times \nabla_i \quad \text{and} \quad \mathbf{l}_{iN,u} = -\mathrm{i}\mathbf{r}_{iN} \times \nabla_i
\end{aligned}
$$

N represents an arbitrary nucleus located in the QC at $\mathbf{r}_N$ and $u, v \in \{1, 2, 3\}$ are tensor component indices. r_{iO} and r_{iN} are the distances of electron i from the origin of the external vector potential and from nucleus N, respectively. $E_{eQC}, 0$ and E_{eQC}, n are the energies of the ground state $\Psi_{eQC,0}$ and the n-th excited state $\Psi_{eQC,n}$, respectively, and “*c.c.*” indicates the complex conjugate of the previous sum. If the outer part is represented by point charges, it has no *direct* effect on $\overleftrightarrow{\sigma}^N$, because the (static) point charges do not induce a magnetic field at any point in space. However, the OP interacts with the QC via the second and the third term in (S6), and exerts an *indirect* effect on the magnetic shielding due to a distortion of the WF. The corresponding shielding that is obtained from Ψ_{eQC} is denoted as $\overleftrightarrow{\sigma}^N_{eQC}$.

The *direct* effect of the OP on the QC can be estimated by calculating the induced magnetic field at $\mathbf{r}_N$ using the WF Ψ_{OP}. This is possible by nucleus-independent chemical shift (NICS) calculations[16] and therefor we label this shielding contribution $\overleftrightarrow{\sigma}^N_{NICS}$.

The error of the QC approximation with point charges is denoted by $\Delta\overleftrightarrow{\sigma}^N_{eQC}$, the error of the QC approximation with point charges approximation plus NICS correction from the OP by $\Delta\overleftrightarrow{\sigma}^N_{eQC+NICS}$. The quantities are defined as the difference between the respective approximations and the exactly calculated value σ^N

$$
\begin{aligned}
\Delta\overleftrightarrow{\sigma}^N_{eQC} &= \overleftrightarrow{\sigma}^N_{eQC} - \overleftrightarrow{\sigma}^N && \text{(S9)}\\
\Delta\overleftrightarrow{\sigma}^N_{eQC+NICS} &= [\overleftrightarrow{\sigma}^N_{eQC} + \overleftrightarrow{\sigma}^N_{NICS}] - \overleftrightarrow{\sigma}^N && \text{(S10)}
\end{aligned}
$$

In several test calculations (hydrogen fluoride dimer in various alignments and intermolecular distances, benzene, the tricyclophosphate anion and rare gas atoms) we found $|\overleftrightarrow{\sigma}^{N}_{NICS}| \ll |\overleftrightarrow{\sigma}^{N}_{eQC}|$ for usual distances, so that $\Delta\overleftrightarrow{\sigma}^{N}_{eQC} \approx \Delta\overleftrightarrow{\sigma}^{N}_{eQC+NICS}$. For non-delocalized systems $\overleftrightarrow{\sigma}^{N}_{NICS}$ usually falls off rapidly and can be omitted in many cases. We will not show all data from these calculations[†] but rather focus on atomic shielding contributions which give hints to the usage of pseudo potentials (PPs) in embedded cluster calculations. Figure S2 shows NICS values $\sigma^{Rg}_{NICS}(r)$ for rare gas atoms (Rg) up to Rn in a range of nuclear distances $r \in [0, 6]$ Å. Calculations were performed at mPW1PW/cc-pV5Z level, unless noted otherwise. $\sigma^{Rg}_{NICS}(r = 0)$ is identical to the nuclear magnetic shielding σ^{Rg}. To a good approximation an exponential decay of $\sigma^{Rg}_{NICS}(r)$ is found at distances $r > r_{vdW}$ ($r_{vdW} \equiv$ *van der Waals* distance).

If PPs are used in NMR calculations at neighboring atoms with a distance r from the the nucleus of interest, the $\sigma^{Rg}_{NICS}(r)$ values may be viewed as (rough) correction increments for the direct core electron contributions of the pseudized atoms. Table S1 gives a list of critical distances r_c at which σ^{Rg}_{NICS} falls below 0.1 or 0.01 ppm. Up to the seventh period all inner shell contributions of atoms are negligible ($\sigma^{Rg}_{NICS} < 0.01$ ppm), if the pseudo atoms are located at distances $r > 3.7$ Å from the nucleus of interest. For atoms of the second period the critical distance reduces to $r = 2.0$ Å. At typical bond distances the inner shell contribution of a neighboring pseudo atom cannot be neglected. This has practical implications for calculations with PPs. Without inner shell corrections, PPs should not be used on atoms in immediate neighborhood to the nucleus of interest. Usage of PPs in the second coordination sphere introduce a small error and usage of PPs in the third or higher coordination spheres around the nucleus of interest is usually unproblematic.

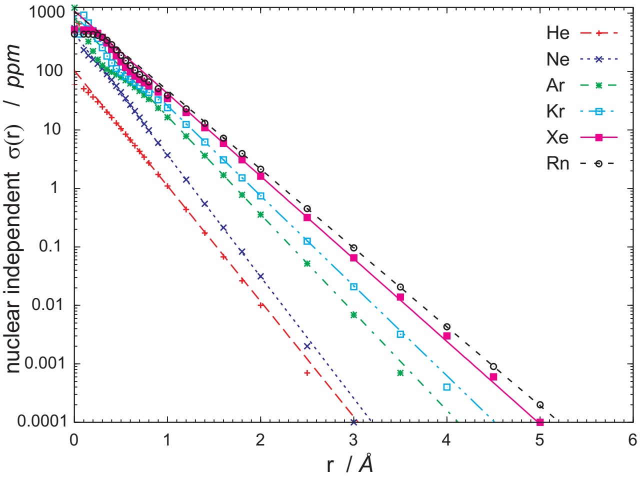

Figure S2: Nucleus independent chemical shift of rare gas atoms at various distances r from the nucleus.

[†] The data will be presented in a forthcoming article.

Table S1: Critical distances r_c of rare gas atoms at which σ_{NICS}^{Rg} falls below a threshold of c ppm.

critical distance [threshold condition]	atom He	 Ne	 Ar	 Kr	 Xe	 Rn
$r_{0.1\,\mathrm{ppm}}/\mathrm{Å}$	1.52	1.76	2.45	2.55	2.79[a]	2.97[a]
$r_{0.01\,\mathrm{ppm}}/\mathrm{Å}$	2.00	2.45	2.76	3.15	3.59[a]	3.69[a]
$r_{vdW}(Rg)/\mathrm{Å}$	1.40	1.54	1.88	2.02	2.16	-

[a] calculated with the cc-PV5Z-PP set (relativistic small core PP + BF)

In summary we find that the electrostatic approximation is acceptable for long distant interactions (above 5Å for non-bonded atoms[17]) while it breaks down at shorter distances where quantum effects like chemical bonding and Pauli repulsion between electrons take place and where direct contributions from the OP region cannot be neglected any more.

S2 Crystal structures and quantum clusters used in this work

S2.1 Crystal structure of $Mg_2P_4O_{12}$

The crystal structure of magnesium cyclotetraphosphate, $Mg_2P_4O_{12}$, has been described by Nord and Lindberg[18]. The tetraphosphate rings $[P_4O_{12}]^{4-}$ in half-chair conformation attain inversion symmetry (C_i=$\bar{1}$) and contain two times the two independent crystallographic P sites (P1,P2) and the six independent O sites (O1–O6). Each P- and O-site occurs eight times in the unit cell. Two independent Mg sites are present (Mg1,Mg2), each occurring four times in the unit cell. The unit cell is shown in Fig. S3. Structure data and labelling of atoms was taken from the ICSD data base[19].

Various clusters were constructed with the sum formula $[P_4O_{12}]^{4-}$, $[Mg_2P_4O_{12}]_1^0$, $[Mg_2P_4O_{12}]_3^0$, $[Mg_2P_4O_{12}]_5^0$, $[Mg_2P_4O_{12}]_7^0$, $[Mg_2P_4O_{12}]_{13}^0$. The last two are shown in Fig. S4. Important parameters of the cluster setup are given in Tab. S2. The result of calculation 8b is given in Tab. 1.

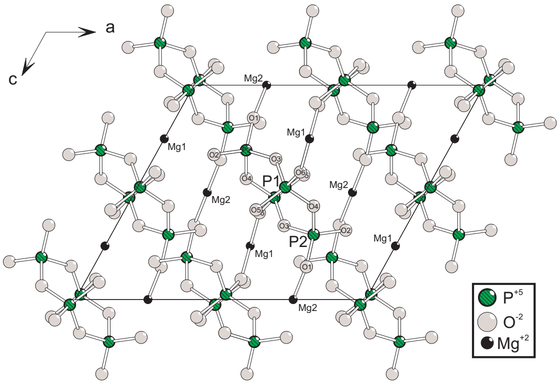

Figure S3: Crystal structure of the $Mg_2P_4O_{12}$ viewed along the *b* axis.

Table S2: Setup of cluster calculations for $Mg_2P_4O_{12}$.

Calc.	Cluster definition		
No	QC	type[a]	setup[b]
1	$[P_4O_{12}]^{4-}$ (Fig. 7a)	NE	mPW1PW/6-311G(3df,3pd)level
2	$[P_4O_{12}]^{4-}$ (Fig. 7a)	EIM	mPW1PW/6-311G(3df,3pd) level; N_a=N_b=N_c=6, $\lfloor N_1 + N_2 \rfloor$= 500, N_{rcp}=1500
3	$[Mg_2P_4O_{12}]^0_1$ (Fig. 7b)	NE	mPW1PW/6-311G(3df,3pd) level
4	$[Mg_2P_4O_{12}]^0_1$ (Fig. 7b)	EEIM	mPW1PW/6-311G(3df,3dp) level; N_a=N_b=N_c=6, $\lfloor N_1 + N_2 \rfloor$= 500, N_{rcp}=1000
5	$[Mg_2P_4O_{12}]^0_3$ (Fig. 7c)	NE	mPW1PW level, 6-311G(3df,3dp) basis for atoms with $0 \leq r_p <$ 2.5 Å, 6-31G(d,p) basis at $r_p \geq 2.5$ Å
6	$[Mg_2P_4O_{12}]^0_3$ (Fig. 7c)	EEIM	mPW1PW level, 6-311G(3df,3dp) basis for atoms with $0 \leq r_p <$ 2.5 Å, 6-31G(d,p) basis at $r_p \geq 2.5$ Å; N_a=N_b=N_c=6, $\lfloor N_1 + N_2 \rfloor$= 600, N_{rcp}=1200
7a	$[Mg_2P_4O_{12}]^0_5$ (Fig. 7d)	NE	mPW1PW level, 6-311G(3df,3dp) basis for atoms with $0 \leq r_p <$ 2.5 Å, 6-31G(d,p) basis at $r_p \geq 2.5$ Å
7b	$[Mg_2P_4O_{12}]^0_5$ (Fig. 7d)	NE	mPW1PW level, 6-311G(3df,3dp) basis for atoms with $0 \leq r_p <$ 2.5 Å, 6-31G(d,p) basis at $2.5 \leq r_p < 5.0$Å, CEP-4G basis at $r_P \geq 5.0$Å supplemented with a *d* function (exponent:0.55 a_0) at P atoms in the range $5.0 \leq r_p < 6.9$Å
8a	$[Mg_2P_4O_{12}]^0_5$ (Fig. 7d)	EEIM	mPW1PW level, 6-311G(3df,3pd) basis for atoms with $0 \leq r_p <$ 2.5 Å, 6-31G(d,p) basis at $r_p \geq 2.5$ Å; N_a=N_b=N_c=6, $\lfloor N_1 + N_2 \rfloor$=1000, N_{rcp}=2000
8b	$[Mg_2P_4O_{12}]^0_5$ (Fig. 7d)	EEIM	as calc. 8a, except 6-31G(d,p) basis at $2.5 \leq r_p < 5.0$Å, CEP-4G basis at $r_P \geq 5.0$Å supplemented with a *d* function (exponent:0.55 a_0) at P atoms in the range $5.0 \leq r_p < 6.9$Å
8c	$[Mg_2P_4O_{12}]^0_5$ (Fig. 7)	EEIM	as calc. 8a, except 6-311++G(3df,3pd) basis is used for atoms with $0 \leq r_p < 2.5$ Å
9	$[Mg_2P_4O_{12}]^0_7$ (Fig. S4a)	NE	mPW1PW level, 6-311G(3df,3pd) basis for 0≤ r_P <2.5Å, 6-31G(d,p) at 2.5≤ r_P <5.0Å, CEP-4G basis at r_P ≥5.0 supplemented with *d* function on P in the range 5.0≤ r_P <6.9Å

(continued on next page)

Tab. S2: *(continued)*

Calc.	Cluster definition		
No	QC	type[a]	setup[b]
10	$[Mg_2P_4O_{12}]^0_7$ (Fig. S4a)	EEIM	mPW1PW level, 6-311G(3df,3pd) basis for atoms with 0≤ r_P <2.5Å, 6-31G(d,p) basis at 2.5≤ r_P <5.0Å, CEP-4G basis at r_P ≥5.0 supplemented with *d* function on P in the range 5.0≤ r_P <6.9Å; N_a=N_b=N_c=5, $\lfloor N_1 + N_2 \rfloor$=700, N_{rcp}=2000
11	$[Mg_2P_4O_{12}]^0_{13}$ (Fig. S4b)	NE	mPW1PW level, 6-311G(3df,3pd) basis for atoms with 0≤ r_P <2.5Å, 6-31G(d,p) basis at 2.5≤ r_P <5.0Å, CEP-4G basis at r_P ≥5.0Å supplemented with *d* function on P in the range 5.0≤ r_P <6.9Å
12	$[Mg_2P_4O_{12}]^0_{13}$ (Fig. S4b)	EEIM	mPW1PW level, 6-311G(3df,3pd) basis for atoms with 0≤ r_P <2.5Å, 6-31G(d,p) basis at 2.5≤ r_P <5.0Å, CEP-4G basis at r_P ≥5.0Å supplemented with *d* function on P in the range 5.0≤ r_P <6.9Å; N_a=N_b=N_c=6, $\lfloor N_1 + N_2 \rfloor$= 700, N_{rcp}=2000

[a] NE=non-embedded calculation, EIM=traditional embedded ion method, EEIM=extended embedded ion method.

[b] r_P is the shortest distance of an atom to one of the four central P atoms.

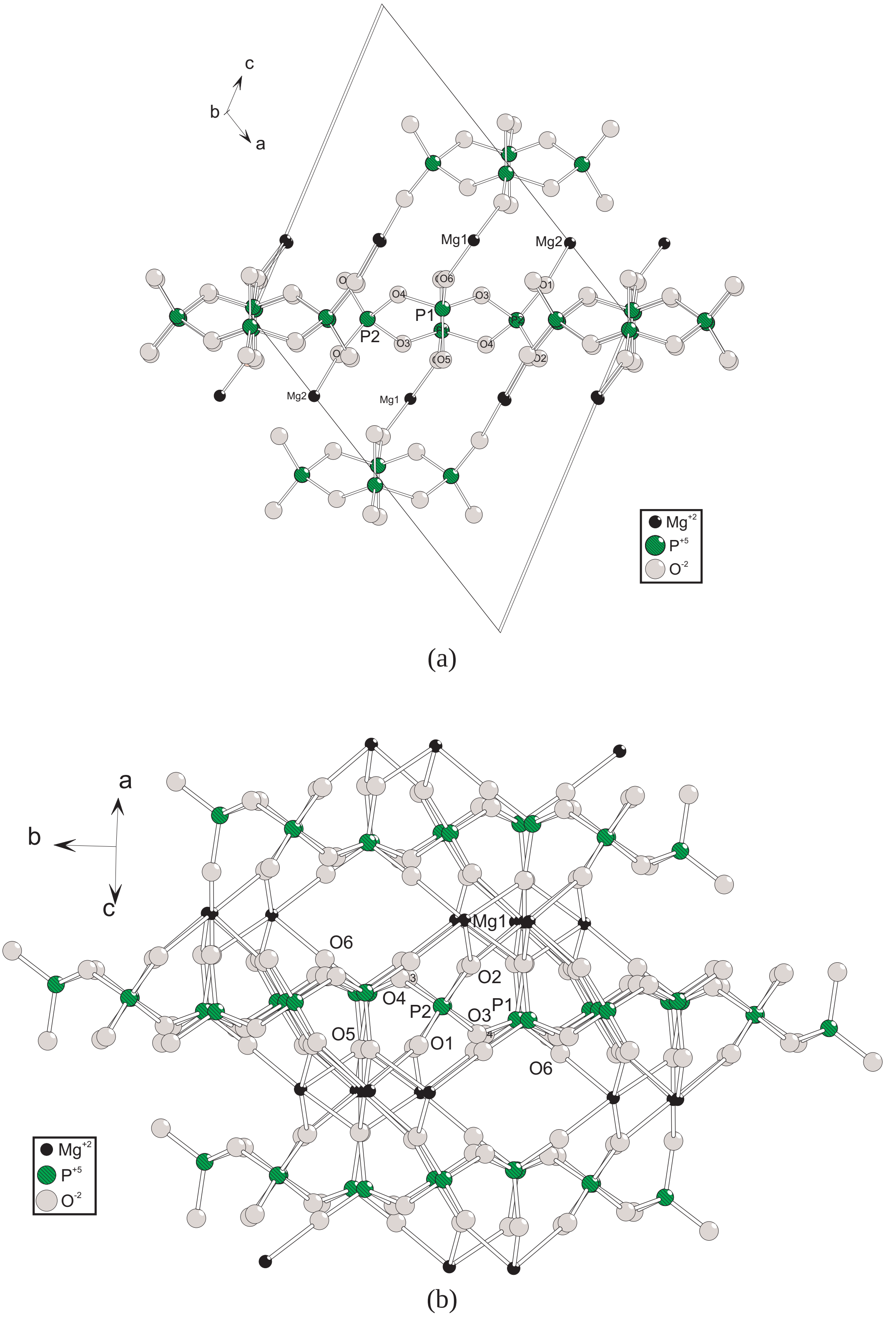

(a)

(b)

Figure S4: Further $Mg_2P_4O_{12}$ clusters. (a): $[Mg_2P_4O_{12}]^0_7$, (b): $[Mg_2P_4O_{12}]^0_{13}$. P sites with off-centerd labels indicate reference points for the local expansion.

S2.2 Crystal structure of α-$Mg_3(PO_4)_2$

The crystal structure of α-magnesium phosphate, α-$Mg_3(PO_4)_2$, has been described by Nord and Kierkegaard[1]. Structure data and site labelling was adopted from[19]. The unit cell is shown in Fig. S5. It contains the seven sites Mg1, Mg2, P1, O1, O2, O3, O4 with the frequencies 4, 2, 4, 4, 4, 4, 4, respectively. The crystal is composed of $[PO_4]^{3-}$ anions (Q_0-phosphate) surrounded by seven Mg^{2+} cations in the next coordination sphere. The P-O bond lengths within an orthophosphate ion increase in the row d(P1-O2)=1.5076Å, d(P1-O4)=1.5273Å, d(P1-O3)=1.5344Å, d(P1-O4)=1.5349Å. Details of the cluster setup are given in Tab. S3. The result of calculation 18 is given in Tab. 1.

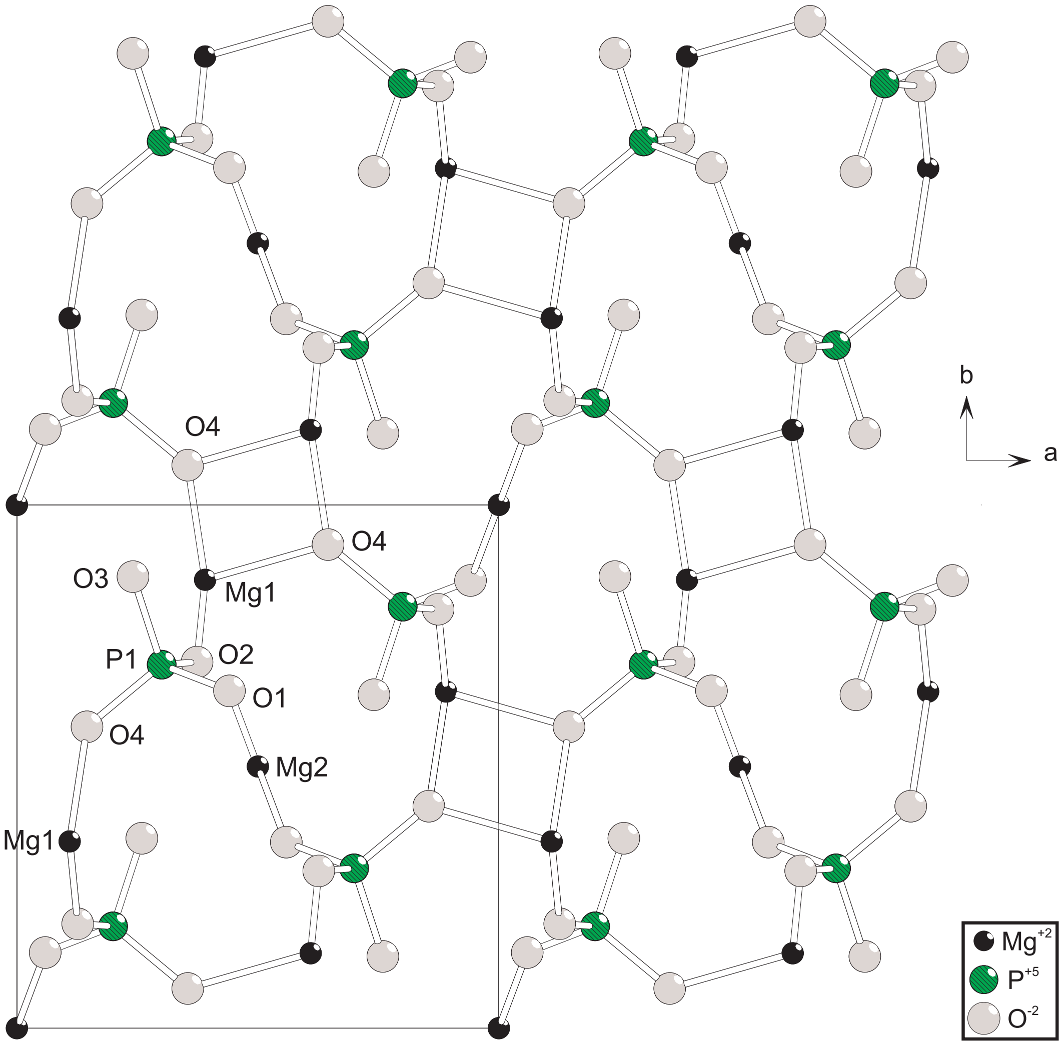

Figure S5: Crystal structure of α-$Mg_3(PO_4)_2$ as reported in[1], 2x2x2 unit cells viewed along *c* axis.

Table S3: Setup of cluster calculations on α-$Mg_3(PO_4)_2$.

Calc.	Cluster definition		
No	QC	type[a]	setup[b]
13	$[PO_4]^{3-}$ (Fig. 9a)	NE	mPW1PW/6-311G(3df,3pd) level
14	$[PO_4]^{3-}$ (Fig. 9a)	EIM	mPW1PW/6-311G(3df,3pd) level; N_a=N_b=N_c=6, $\lfloor N_1 + N_2 \rfloor$= 500, N_{rcp}=2000
15	$[Mg_3(PO_4)_2]^0_1$ (Fig. 9b)	NE	mPW1PW/6-311G(3df,3pd) level
16	$[Mg_3(PO_4)_2]^0_1$ (Fig. 9b)	EEIM	mPW1PW/6-311G(3df,3dp) level; N_a=N_b=N_c=7, $\lfloor N_1 + N_2 \rfloor$= 700, N_{rcp}=2000
17	$[Mg_3(PO_4)_2]^0_5$ (Fig. 9c)	NE	mPW1PW level, 6-311G(3df,3pd) basis at $0.0 \leq r_P < 2.5$Å, 6-31G(d,p) basis at $2.5 \leq r_P < 5.0$Å, CEP-4G PP + basis at $r_P \geq 5.0$Å augmented with a d function (exponent=0.55 a_0) at P atoms; calculation not converged
18	$[Mg_3(PO_4)_2]^0_5$ (Fig. 9c)	EEIM	mPW1PW level, 6-311G(3df,3pd) basis at $0.0 \leq r_P < 2.5$Å, 6-31G(d,p) basis at $2.5 \leq r_P < 5.0$Å, CEP-4G PP + basis at $r_P \geq 5.0$Å augmented with a single d function (exponent= 0.55 a_0) at P atoms; N_a=N_b=N_c=7, $\lfloor N_1 + N_2 \rfloor$= 700, N_{rcp}=2000
19	$[Mg_3(PO_4)_2]^0_8$ (Fig. 9d)	NE	mPW1PW level, 6-311G(3df,3dp) basis at $0 \leq r_{P,O1,O2,O3,O4} <$ 2.1Å, 6-31G(d,p) at $2.1 \leq r_{P,O1,O2,O3,O4} < 3.1$Å, CEP-4G PP + basis elsewhere augmented with a single d function (exponent= 0.55 a_0) on P-atoms in the range $3.1 \leq r_{P,O1,O2,O3,O4} < 6.9$Å; calculation not converged
20	$[Mg_3(PO_4)_2]^0_8$ (Fig. 9d)	EEIM	mPW1PW level, 6-311G(3df,3pd) basis for $0 \leq r_{P,O1,O2,O3,O4} <$ 2.1Å, 6-31G(d,p) at $2.1 \leq r_{P,O1,O2,O3,O4} < 3.1$Å, CEP-4G PP + basis elsewhere augmented with a single d function (exponent= 0.55 a_0) on P-atoms in the range $3.1 \leq r_{P,O1,O2,O3,O4} < 6.9$Å; N_a=N_b=N_c=7, $\lfloor N_1 + N_2 \rfloor$= 700, N_{rcp}=2000

[a] NE=non-embedded calculation, EIM=traditional embedded ion method, EEIM=extended embedded ion method.

[b] r_P is the shortest distance of an atom to the central P atom, $r_{P,O1,O2,O3,O4}$ is the shortest distance to one of the atoms of the central $[PO_4]^{3-}$ group.

S2.3 Crystal structure of α-$Mg_2P_2O_7$

Crystal structures of α-$Mg_2P_2O_7$ have been reported by Calvo[20] and Łukaszewicz[21]. The space group symmetry was determined to $B2_1/c$ (no 14) in both works, but significant differences appear in some bond parameters, which has a significant effect on calculated NMR results. In addition, the two works differ in the choice of the unit cell and in the labelling of crystallographic sites. For comparison of the two crystal structures we juxtaposed bond parameters of equivalent sites in Tab. S4.

Table S4: Comparison of selected bonding parameters in the α-$Mg_2P_2O_7$ crystal as reported in the X-ray diffraction works of Calvo[20] and Łukaszwicz[21].

bonding parameter[a]	Calvo[b]	Łukaszewicz[c]
atomic distances in Å		
P1–O4 (P1–O7)	1.473(18)	1.482(23)
P1–O3 (P1–O5)	1.506(14)	1.559(18)
P1–O7 (P1–O3)	1.535(99)	1.548(10)
P1–O1 (P1–O1)	1.613(44)	1.630(15)
P2–O6 (P2–O4)	1.521(8)	1.553(23)
P2–O5 (P2–O6)	1.526(19)	1.489(19)
P2–O2 (P2–O2)	1.535(93)	1.525(12)
P2–O1 (P2–O1)	1.568(20)	1.604(14)
Mg1(a)–O3 (Mg2(a)–O5)	2.059(68)	2.004(17)
Mg1(b)–O3 (Mg2(b)–O5)	2.137(71)	2.111(14)
Mg1–O7 (Mg2–O3)	2.072(46)	2.068(27)
Mg1–O2 (Mg2–O2)	2.085(53)	2.090(23)
Mg1–O5 (Mg2–O6)	2.135(74)	2.154(15)
Mg1–O6 (Mg2–O4)	2.143(67)	2.115(20)
Mg2–O4 (Mg1–O7)	1.984(59)	1.950(29)
Mg2–O5 (Mg1–O6)	2.025(79)	2.019(30)
Mg2–O7 (Mg1–O3)	2.036(60)	2.014(35)
Mg2–O2 (Mg1–O2)	2.054(36)	2.057(47)
Mg2–O6 (Mg1–O4)	2.120(67)	2.114(42)
bond angles in deg		
P1–O1–P2 (P1–O1–P2)	143.98(29)	140.18(76)
O1–P1–O3 (O1–P1–O5)	104.89(22)	102.61(69)
O1–P1–O4 (O1–P1–O7)	109.52(29)	110.87(85)
O1–P1–O7 (O1–P1–O3)	102.72(22)	101.24(62)
O1–P2–O2 (O1–P2–O2)	107.65(22)	106.65(65)
O1–P2–O5 (O1–P2–O6)	102.23(22)	100.10(74)
O1–P2–O6 (O1–P2–O4)	110.25(27)	110.97(86)
P1–O3–Mg1(a) (P1–O5–Mg2(a))	128.68(28)	127.89(91)
P1–O3–Mg1(b) (P1–O5–Mg2(b))	127.69(28)	126.04(76)
P1–O4–Mg2 (P1–O7–Mg1)	155.26(39)	156.22(119)
P1–O7–Mg1 (P1–O3–Mg2)	131.53(24)	129.87(76)
P1–O7–Mg2 (P1–O3–Mg1)	129.09(24)	129.82(100)
P2–O2–Mg1 (P2–O2–Mg2)	132.43(24)	132.51(79)
P2–O2–Mg2 (P2–O2–Mg1)	128.23(23)	128.09(115)
P2–O5–Mg1 (P2–O6–Mg2)	124.39(27)	128.67(79)
P2–O5–Mg2 (P2–O6–Mg1)	129.44(25)	125.32(100)
P2–O6–Mg1 (P2–O4–Mg2)	144.79(20)	145.33(111)
P2–O6–Mg2 (P2–O4–Mg1)	113.62(25)	111.80(88)
dihedral angles in deg		
O4–P1–O1–P2 (O7–P1–O1–P2)	10.19(68)	12.50(208)
O5–P2–O1–P1 (O6–P2–O1–P1)	169.57(55)	168.28(166)
O1–P1–O3–Mg1(a) (O1–P1–O5–Mg2(a))	-24.27(42)	-26.66(131)

(continued on next page)

Tab. S4: *(continued)*

bonding parameter[a]	Calvo[b]	Łukaszewicz[c]
O1–P1–O3–Mg1(b) (O1–P1–O5–Mg2(b))	170.58(32)	170.45(101)
O1–P1–O4–Mg2 (O1–P1–O7–Mg1)	16.15(99)	16.95(414)
O1–P1–O7–Mg1 (O1–P1–O3–Mg2)	92.22(39)	96.61(153)
O1–P1–O7–Mg2 (O1–P1–O3–Mg1)	-78.19(39)	-77.69(210)
O1–P2–O2–Mg1 (O1–P2–O2–Mg2)	-107.93(38)	110.16(141)
O1–P2–O2–Mg2 (O1–P2–O2–Mg1)	-55.51(41)	-53.68(197)
O1–P2–O5–Mg1 (O1–P2–O6–Mg2)	-173.19(33)	-173.85(110)
O1–P2–O5–Mg2 (O1–P2–O6–Mg1)	-20.36(39)	-23.02(181)
O1–P2–O6–Mg1 (O1–P2–O4–Mg2)	7.77(59)	9.2(22)
O1–P2–O6–Mg2 (O1–P2–O4–Mg1)	162.69(26)	162.16(139)

[a] site labels according to ICSD entry 15326 (Calvo). Labels in parenthesis according to ICSD 30434 (Łukaszewicz).
[b] taken from ICSD database[19], entry 15326
[c] taken from ICSD database[19], entry 30434

In this work the probably more reliable structure of Calvo, ICSD entry 15326[19], is used as well as the site labelling given there. The crystal structure is shown in Fig. S6. Two independent P-sites (P1,P2), seven O-sites (O1–O7) and two Mg-sites (Mg1,Mg2) are present, all of which are on general crystallographic positions (Wyckoff index 8*e*). Each pyrophosphate $[P_2O_7]^{4-}$ unit contains all P- and O-sites exactly for one time. O1 is the bridging atom between P1 and P2 with a shorter bond to P2. Of the terminal oxygens O4 is special in the sense that it has the shortest P-O distance (1.473Å), the shortest O-Mg distance (1.984Å) and that it is only coordinated by a single Mg atom (Mg2). The remaining oxygens are coordinated by two Mg sites. Of these oxygens O3 is coordinated to two Mg1 sites, whereas all others are coordinated to one Mg1 and one Mg2. Note, that the P_2O_7-unit extended by the coordinated Mg atoms is a chiral fragment and that both enantiomers of that fragment are present in the crystal. The coordination number for the Mg1 cation is six, but only five for Mg2. The setup for various cluster calculations is shown in Fig. S5. The result of calculation 24 is shown in Tab. 1.

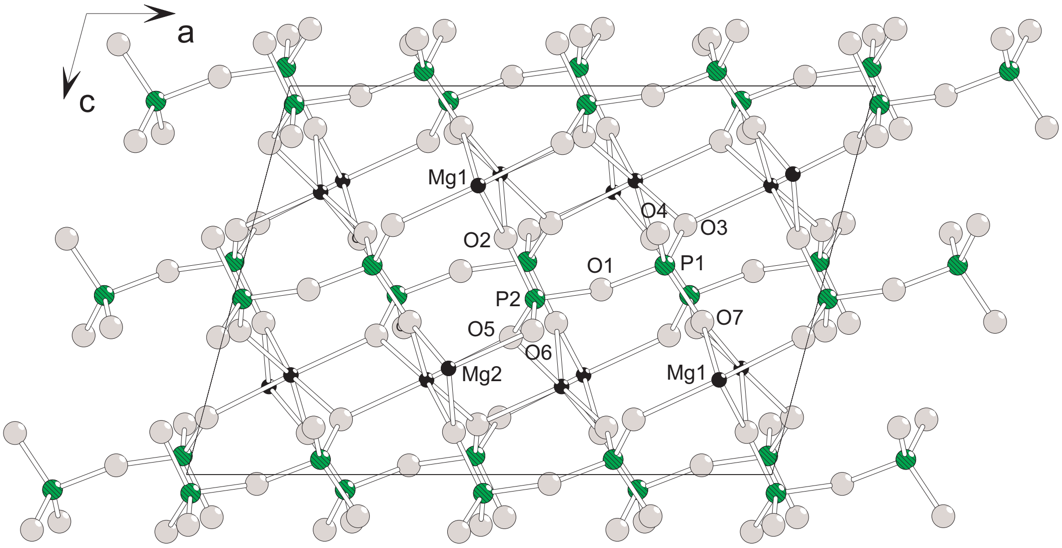

Figure S6: Unit cell of α-$Mg_2P_2O_7$ viewed along b axis.

Table S5: Setup of cluster calculations on α-$Mg_2P_2O_7$.

Calc.	Cluster definition		
No	QC	type[a]	setup[b]
21	$[P_2O_7]^{4-}$ (Fig. 10a)	NE	structure from[20]; mPW1PW/6-311G(3df,3pd)level
22	$[P_2O_7]^{4-}$ (Fig. 10a)	EIM	structure from[20]; mPW1PW/6-311G(3df,3pd) level, N_a=N_b=N_c=5, $\lfloor N_1 + N_2 \rfloor$= 600, N_{rcp}=1500
23	$[Mg_2P_2O_7]^0_9$ (Fig. 10b)	NE	structure from[20]; mPW1PW level, 6-311G(3df,3pd) basis at $0 \leq r_P < 2.5$Å, 6-31G(d,p) at $2.5 \leq r_P < 5$Å, CEP-4G at $r_P \geq 5$Å augmented with d-functions (exp=0.55 a_0) on P in the range $5 \leq r_P < 8$Å
24	$[Mg_2P_2O_7]^0_9$ (Fig. 10b)	EEIM	structure from[20]; mPW1PW level, 6-311G(3df,3pd) basis at $0 \leq r_P < 2.5$Å, 6-31G(d,p) at $2.5 \leq r_P < 5$Å, CEP-4G at $r_P \geq 5$Å augmented with d-functions (exp=0.55) on P in the range $5 \leq r_P < 8$Å, N_a=N_b=N_c=6, $\lfloor N_1 + N_2 \rfloor$= 700 N_{rcp}=2000
25	$[Mg_2P_2O_7]^0_9$	EEIM	as calc. 24, but structure taken from[21]

[a] NE=non-embedded calculation, EIM=traditional embedded ion method, EEIM=extended embedded ion method.

[b] r_P is the shortest distance of an atom to one of the two central P atoms.

S2.4 Crystal structure of MgP_4O_{11}

The crystal structure of magnesium ultraphosphate has been reported by Stachel *et al.*[22]. The unit cell is shown in Fig. S7. Details of the quantum cluster setup are listed in Tab. S6. The results of calculations 27 and 29 are given in Tab. 1.

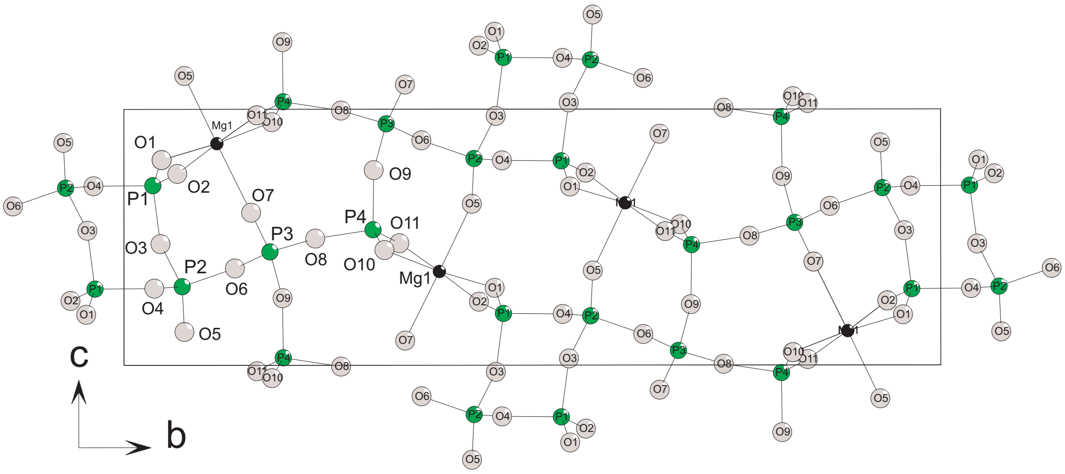

Figure S7: Unit cell of MgP_4O_{11} viewed along the *a* axis.

Table S6: Setup of cluster calculations on MgP_4O_{11}.

Calc. No	Cluster definition		
	QC	type[a]	setup[b]
26	$[MgP_4O_{11}]^0_6$ (Fig. 11a)	NE	mPW1PW level, 6-311G(3df,3pd) basis at $0 \leq r_{P1,P2} < 2.5$Å, 6-31G(d,p) basis at $2.5 \leq r_{P1,P2} < 5$Å, CEP-4G basis at $r_{P1,P2} \geq 5$Å augmented with *d*-function on P in the range $5 \leq r_{P1,P2} < 8$Å; calculation not converged
27	$[MgP_4O_{11}]^0_6$ (Fig. 11a)	EEIM	mPW1PW level, 6-311G(3df,3pd) basis at $0 \leq r_{P1,P2} < 2.5$Å, 6-31G(d,p) basis at $2.5 \leq r_{P1,P2} < 5$Å, CEP-4G basis at $r_{P1,P2} \geq 5$Å augmented with *d*-function on P in the range $5 \leq r_{P1,P2} < 8$Å; N_a=N_c=6, N_b=3, $\lfloor N_1 + N_2 \rfloor$=600, N_{rcp}=2200
28	$[MgP_4O_{11}]^0_5$ (Fig. 11b)	NE	6-311G(3df,3pd) basis for atoms with $0 \leq r_{P3,P4} < 3.1$Å, 6-31G(d,p) at $3.1 \leq r_{P3,P4} < 4.1$Å, CEP-4G augmented with d-functions on P atoms at $r_{P3,P4} \geq 4.1$Å
29	$[MgP_4O_{11}]^0_5$ (Fig. 11b)	EEIM	6-311G(3df,3pd) basis for atoms with $0 \leq r_{P3,P4} < 3.1$Å, 6-31G(d,p) at $3.1 \leq r_{P3,P4} < 4.1$Å, CEP-4G augmented with d-functions on P atoms at $r_{P3,P4} \geq 4.1$Å; N_a=N_c=7, N_b=4, $\lfloor N_1 + N_2 \rfloor$=600, N_{rcp}=2400

[a] NE=non-embedded calculation, EEIM=extended embedded ion method.

[b] $r_{P\alpha,P\beta}$ is the shortest distance of an atom to one of the two central P atoms.

S3 Calculation details for the ^{31}P $\sigma \leftrightarrow \delta$ calibration curve

In the following subsections details to the calculated and experimental data are listed that is used for establishing the conversion equation from the absolute shielding scale to the experimental chemical shift scale. Both, theoretical and experimental data, possess a limited accuracy, only: Theoretical data suffers from various approximations that are made to make the calculations feasible. We mention here the neglect of vibrational motions (r_e-structures), inaccurate treatment of electron correlation or intermolecular effects, which all can have a significant effect on the NMR parameters[23]. Experimental data on the other side suffer from experimental errors, such as deviations of up to 2 ppm in early field-sweep spectrometers[24]. In modern spectrometers such apparatus-related errors can be routinely diminished below 0.1 ppm. Here, the main source of “error” results in many cases from an inexact description of the experimental conditions. E.g. the solvent dependency (either by change of magnetic susceptibility or by intermolecular effects on the sample and the reference compound) or the temperature (introducing molecular vibrations) are well known sources that lead to variation of NMR parameters. Nevertheless, this additional information is often omitted for brevity in tabulated NMR parameters[24–26]. Solvent effects of more than 4 ppm have been observed for ^{31}P chemical shifts[27,28] in usual liquids. A special case is the P_4 molecule for which a shift variation of 92 ppm depending on the environment has been reported[26].

In some works, the definition of the chemical shift is not clearly specified which is problematic as the definition changed over the years from

$$\delta = \frac{H_s - H_{ref}}{H_{ref}} \cdot 10^6 = \frac{\nu_{ref} - \nu_s}{\nu_{ref}} \cdot 10^6 \text{ in most works before 1972, e.g.}^{24} \qquad \text{(S11)}$$

over

$$\delta = \frac{\nu_s - \nu_{ref}}{\nu_{ref}} \cdot 10^6 \text{ (IUPAC Recommendation in 1972}^{29,30}\text{)} \qquad \text{(S12)}$$

to

$$\delta = \frac{\nu_s - \nu_{ref}}{\nu_{ref}} \text{ (IUPAC Recommendation in 2001,2008}^{31,32}\text{)} \qquad \text{(S13)}$$

This has lead to considerable confusion in transferring older data into newer compilations. In the following tables we use convention (S13). Unless noted otherwise all cited values from earlier literature are converted silently due to their year of appearance to the most recent convention (S13).

A linear equation is assumed for the conversion between theoretically calculated shieldings and chemical shifts

$$\sigma_{iso,theor} = A + B \cdot \delta_{iso,exp} \qquad \text{(S14)}$$

The parameters A and B in this equation are determined by a least squares fit of a test data set containing 20 different phosphorus compounds: P_4O_{10}, PF_3, PCl_3, OPF_3, $OPCl_3$, PF_5, PCl_5, $PF_4C{\equiv}C\text{-}H$, $PFO_6C_4H_4$, $PClO_3C_2H_4$, $OPCl_2F$, $OPClF_2$, $PClO_3C_3H_6$, $PClO_3C_6H_4$, $PO_4C_4H_7$, PH_3, P_4, P_4O_6, P_4O_7, P_4O_8. This choice is convenient for several reasons. First, we cover the entire chemical shift range of ordinary ^{31}P compounds. Second, all substances are characterized by an experimental structure and by NMR data. Third, most molecules are rather small and symmetric and it is unlikely that intramolecular dynamics has a strong effect on the NMR parameters. Therefore, it is easy to calculate NMR parameters for them at the experimental structures. Detailed information is given in Tab. S7. In addition, we performed NMR calculations at optimized structures, see Tab. S8. Systematic calculations on sets of ^{31}P compounds have been performed in the past already[33–36], but not with our chosen quantum chemical model (mPW1PW)[37].

Table S7: Experimental and calculated NMR shielding parameters of ^{31}P reference compounds at experimental molecular structures.

Compound	Site	δ_{exp}	Shift	Structure	absolute magnetic shielding in ppm at mPW1PW level with various basis sets				
		ppm	Ref.	Ref.	6-31G(d,p)_6D	6-31G(d,p)_5D	6-311G(3df,3pd)	6-311++G(3df,3pd)	6-311++G(d,p)
P_4O_{10}	P1	-46.8	38	39	433.19	434.95	357.92	357.92	371.53
P_4O_{10}	P2	-45.5	38	39	434.39	436.15	359.28	359.28	372.92
P_4O_8	P1	123.8	40	41	252.34	254.59	173.6	173.47	183.48
P_4O_8	P2	-42.2	40	41	432.46	434.07	355.06	354.51	367.18
P_4O_7	P1	-61.0	42,a	43,b	445.85	447.33	368.88	368.29	381.42
P_4O_7	P2	123.5	42,a	43,b	248.33	250.74	166.57	166.61	176.11
P_4O_7	P3	123.5	42,a	43,b	248.96	251.29	167.5	167.52	176.92
P_4O_7	P4	123.5	42,a	43,b	251.43	253.81	169.56	169.59	179.47
P_4O_6	P1	109.5	44,c	45	275.48	277.92	195.22	195.73	206.08
P_4O_6	P2	109.5	44,c	45	262.21	264.73	180.89	181.43	190.42
P_4O_6	P3	109.5	44,c	45	271.17	273.68	190.22	190.75	200.72
P_4O_6	P1	112.5	26,46,d	47	273.68	276.14	192.29	192.79	203.21
PF_3	P1	97.0	24,26,48	49	255.36	256.67	175.91	179.52	179.79
PCl_3	P1	220	24,26,48	49	107.95	107.11	55.28	57.58	59.38
OPF_3	P1	-35.5	24,26,48,50	49	412.43	415.58	337.18	335.67	342.53
$OPCl_3$	P1	2.2	24,26,48	49	335.82	335.67	286.17	283.48	294.30
PF_5	P1	-80.3	26,51	49	429.05	431.30	374.15	372.81	375.60
PF_4CCH	P1	-67.8	52	53	423.84	425.93	367.49	366.52	373.63
$PClO_3C_2H_4$	P1	22.8	26,27	54	347.43	348.34	273.55	271.81	281.27
$OPCl_2F$	P1	0.0	24,26	55	365.26	366.48	301.42	298.77	309.38
$OPClF_2$	P1	-14.8	24,26	55	389.48	391.81	318.27	316.06	325.39
PH_3	P1	-238	24	49	602.36	602.55	575.8	575.35	580.73
P_4	P1	-488	24,26,56	49	856.85	857.77	857.57	857.93	861.48

[a] taken from solid state spectrum at T=258 K in Fig.7 of that work.

[b] structure taken from printed version of that work. Structure given in the ICSD data base (entry 49545) is erroneous in O1 coordinate.

[c] solid state data;averaged value of two sites reported in that work.

[d] liquid state data.

Table S8: Experimental and calculated NMR shielding parameters of ^{31}P reference compounds at mPW1PW level with various basis sets. Molecular structures were optimized at the same method/basis set combination.

Compound	Site	$\frac{\delta_{exp}}{\text{ppm}}$	Shift Ref.	Structure Ref.	absolute magnetic shielding in ppm at mPW1PW level with various basis sets			
					6-31G(d,p)_6D	6-31G(d,p)_5D	6-311G(3df,3pd)	6-311++G(3df,3pd)
P_4O_{10}	P1+P2	-46.15	[38,a]	opt	427.34	429.02	359.05	358.41
P_4O_8	P1	123.8	[40]	opt	232.70	235.08	164.73	164.38
P_4O_8	P2	-42.2	[40]	opt	424.53	426.06	355.44	354.61
P_4O_7	P1	-60.5	[40]	opt	445.29	446.75	375.63	375.21
P_4O_7	P2	132.5	[40]	opt	234.24	236.46	161.36	161.32
P_4O_6	P1	112.5	[26,46]	opt	267.80	270.19	190.40	190.83
PF_3	P1	97.0	[24,26,48]	opt	246.45	247.07	175.23	178.03
PCl_3	P1	220	[24,26,48]	opt	78.84	77.98	47.03	48.26
OPF_3	P1	-35.5	[24,26,48,50]	opt	405.05	404.77	336.97	335.3
$OPCl_3$	P1	2.2	[24,26,48]	opt	322.5	322.31	285.64	282.36
PF_5	P1	-80.3	[26,51]	opt	419.13	421.04	372.40	370.64
PF_4CCH	P1	-67.8	[52]	opt	416.4	416.12	367.12	365.79
$PFO_6C_4H_4$	P1	-40.23	[57]	opt	393.81	395.64	342.79	341.81
$PClO_3C_2H_4$	P1	22.8	[26,27]	opt	345.79	346.75	282.85	280.51
$OPCl_2F$	P1	0.0	[24,26]	opt	345.35	346.23	294.83	291.6
$OPClF_2$	P1	-14.8	[24,26]	opt	374.20	376.04	312.80	310.18
$PClO_3C_3H_6$	P1	-2.8	[26,27]	opt	365.54[b]	366.3[b]	303.89[b]	301.98[b]
$PClO_3C_6H_4$	P1	18.4	[26,27]	opt	346.49	347.11	283.80	281.98
$PO_4C_4H_7$	P1	-7.97	[28]	opt	396.77	397.64	326.92	325.14
PH_3	P1	-238	[24]	opt	601.80	602.04	578.11	577.88
P_4	P1	-488	[24,26,56]	opt	870.88	871.93	879.54	878.56

[a] averaged value for P1 and P2 in that work.

[b] averaged values for two ring confomers that are assumed to be in rapid exchange.

All calculations have been performed with the GAUSSIAN 03 program[58]. The calculated isotropic magnetic shieldings ($\sigma_{iso,theor}$) and the experimentally observed isotropic shifts ($\delta_{iso,exp}$) are plotted together with the corresponding fitting curves in Fig. S8. The result of the fit depends on the employed basis set and on the molecular structure used for the calculation. We varied between 6-31G(d,p), 6-311G(3df,3pd), and 6-311++G(3df,3pd) basis sets. By default the 6-31G(d,p) basis set uses six cartesian functions to represent the angular part of the *d* orbitals (6D). We also used this basis in combination with five spherical harmonic functions (5D). Except from experimentally determined structures, we used also quantum chemically optimized ones, employing the same basis set that is used in the subsequent calculation of NMR parameters. This results in different sets of fitted parameters which are collected in Tab. S9.

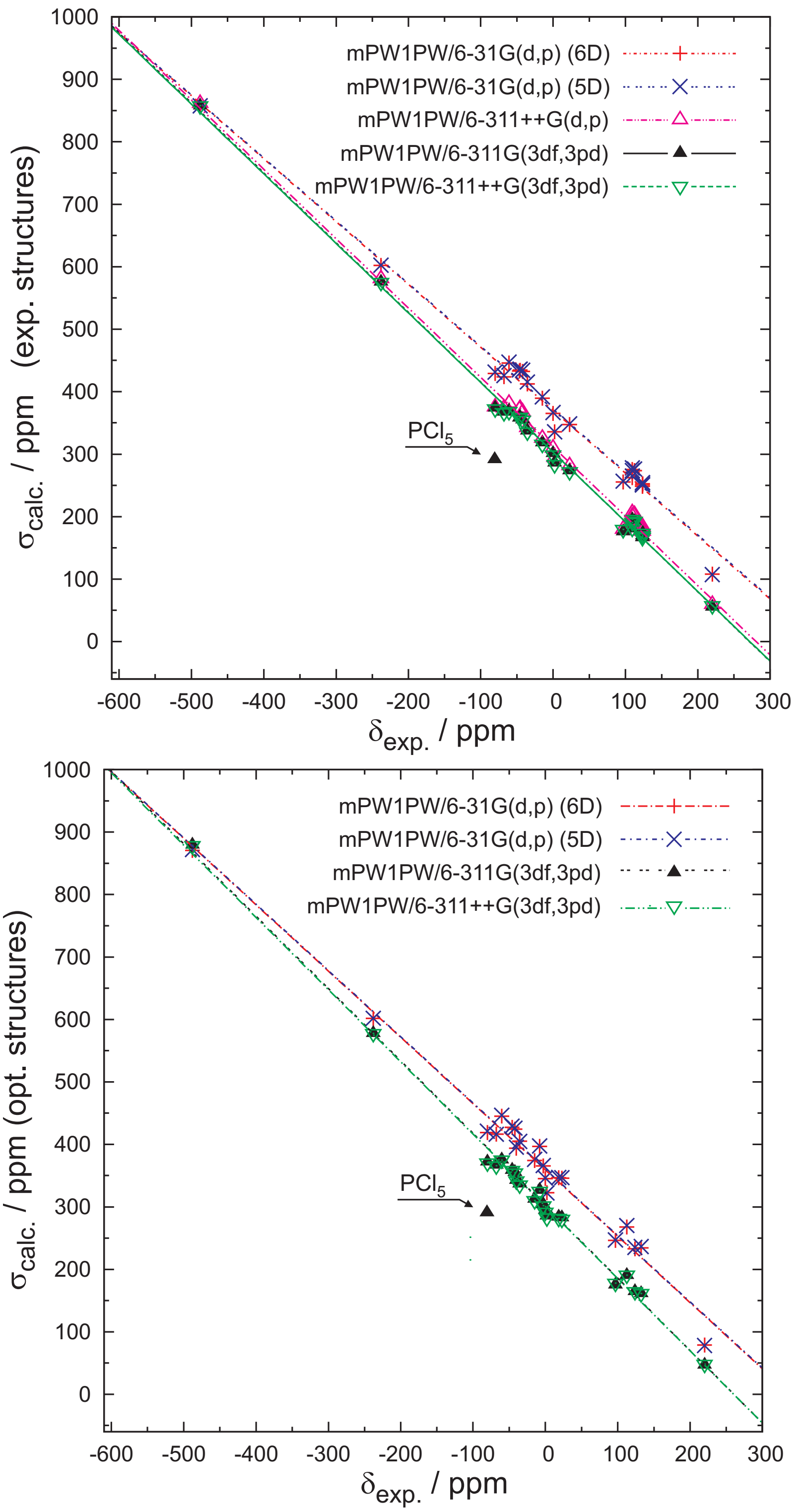

Figure S8: Correlation between experimental chemical shifts and calculated magnetic shieldings. *top*: experimental structures were used, *bottom*: quantum chemically optimzed structures were used.

Table S9: Linear Fit of equation $\sigma_{theor} = A + B \cdot \delta_{exp}$ to the experimental data.

basis set	optimized parameters A / ppm	B	standard deviation / ppm (number of data points)
experimental molecular structures used			
6-31G(d,p) 6D	370.17±3.46	-1.0072±0.0239	16.59 (N=23)
6-31G(d,p) 5D	371.87±3.60	-1.0058±0.0248	17.25 (N=23)
6-311++G(d,p)	311.64±2.45	-1.1110±0.0169	11.75 (N=23)
6-311G(3df,3pd)	303.29±2.00	-1.1174±0.0137	9.56 (N=23)
6-311++G(3df,3pd)	302.99±2.06	-1.1147±0.0142	9.88 (N=23)
quantum chemically optimized molecular structures			
6-31G(d,p) 6D	359.13±4.56	-1.0613±0.0322	20.70 (N=21)
6-31G(d,p) 5D	360.16±4.68	-1.0609±0.0330	21.24 (N=21)
6-311G(3df,3pd)	301.84±2.43	-1.1589±0.0172	11.03 (N=21)
6-311++G(3df,3pd)	300.86±2.50	-1.1564±0.0177	11.37 (N=21)

PCl_5 turns out to be problematic in the fit procedure. Either the experimental data are wrong, or the molecule is difficult to treat with our chosen (non-relativistic) quantum chemical model. Relativistic effects are known to have a significant impact on the NMR parameters in phosphorus halides[59]. Hence, we removed PCl_5 from the fitting data set.

Expectedly, the correlation between experimental shifts and calculated shieldings at 6-31G(d,p) level is the worst in the series of calculations. The calculations with 6-311G(3df,3pd) and 6-311++(3df,3pd) basis sets show significantly improved results. The close similarity between the latter two indicates that diffuse basis functions are not necessary for the calculations of the neutral species. Moreover, sufficiently accurate structures can be obtained from optimizations with these bases, as demonstrated by the similarity between NMR parameters at optimized and experimental structures. The usage of a 6-311G(3df,3pd) basis with the mPW1PW functional seems to be a useful compromise between the demand for an accurate basis and economical aspects of the calculations. By default, we use the correlation parameters A, B obtained from calculations at the experimental structures.

When calculating ^{31}P chemical shift anisotropy parameters from theoretically calculated magnetic shielding parameters, we solve eq. (S14) for δ and calculate each chemical shielding tensor eigenvalue according to

$$\delta_{ii,theor} = \frac{\sigma_{ii,theor} - A}{B} \tag{S15}$$

At this we use the basis set specific correlation parameters A and B. From these $\delta_{ii,theor}$ values we calculate the CSA parameters according to the Haeberlen-Mehring-Spiess convention[60].

S4 Full references to abbreviated citations

The references 33, 34, 41 and 42 of the main article were abbreviated due to their length. The corresponding full citations are given as entries[58,61–63] in the following reference list.

References

[1] A. G. Nord and P. Kierkegaard, *Acta Chem. Scand.*, 1968, **22**, 1466–1474.

[2] N. F. Ramsey, *Phys. Rev.*, 1950, **78**, 699–703.

[3] A. Saika and C. P. Slichter, *J. Chem. Phys.*, 1954, **22**, 26–28.

[4] H. M. McConnell, *J. Chem. Phys.*, 1957, **27**, 226–229.

[5] J. A. Pople, *J. Chem. Phys.*, 1962, **37**, 53–59.

[6] J. Mason, *J. Chem. Soc., Faraday Trans. 2*, 1977, **73**, 1464–1474.

[7] C. J. Jameson and A. D. Buckingham, *J. Phys. Chem.*, 1979, **83**, 3366–3371.

[8] C. van Wüllen, in *Calculation of NMR and EPR Parameters - Theory and Applications*, ed. M. Kaupp, M. Bühl and V. G. Malkin, Wiley-VCH, 2004, ch. 6, pp. 85–100.

[9] C. J. Jameson and A. C. de Dios, *J. Chem. Phys.*, 1992, **97**, 417–434.

[10] C. J. Jameson and A. C. de Dios, *J. Chem. Phys.*, 1993, **98**, 2208–2217.

[11] A. Barszczewicz, M. Jaszunski, T. Helgaker and K. Ruud, *Chem. Phys. Lett.*, 1996, **250**, 1–8.

[12] R. A. Hegstrom, *Phys Rev.*, 1979, **A19**, 17–30.

[13] C. J. Pickard and F. Mauri, *Phys. Rev. B*, 2001, **63**, 245101.

[14] D. Sebastiani and M. Parinello, *J. Phys. Chem.*, 2001, **A 105**, 1951–1958.

[15] M. Kaupp, in *Interpretation of NMR Chemical Shifts*, ed. M. Kaupp, M. Bühl and V. G. Malkin, Wiley-VCH, 2004, ch. 18, pp. 293–306.

[16] P. v. R. Schleyer, C. Maerker, A. Dransfeld, H. Jiao and N. J. R. van Eikema Hommes, *J. Am. Chem. Soc.*, 1996, **118**, 6317–6318.

[17] G. G. Hall, *Theor. Chim. Acta*, 1983, **63**, 357–364.

[18] A. Nord and K. B. Lindberg, *Acta. Chem. Scand.*, 1975, **A29**, 1–6.

[19] P. Hewat, *Inorganic Crystal Structure Database (ICSD-for-WWW)*, Fachinformationszentrum Karlsruhe (FIZ), Release 2006-2 edn.

[20] C. Calvo, *Acta Cryst.*, 1967, **23**, 289–295.

[21] K. Łukaszewicz, *Bull. Acad. Pol. Sci. Chim.*, 1967, **15**, 53–57.

[22] D. Stachel, H. Paulus, C. Guenter and H. Fuess, *Z. Kristallogr.*, 1992, **199**, 275–276.

[23] T. Helgaker, M. Jaszuński and K. Ruud, *Chem. Rev.*, 1999, **99**, 293–352.

[24] M. M. Crutchfield, C. H. Dungan, J. H. Letcher, V. Mark and J. R. V. Watzer, *P^{31} Nuclear Magnetic Resonance*, Wiley Interscience, New York, 1967, vol. 5.

[25] N. Muller, P. C. Lauterbur and J. Goldenson, *J. Am. Chem. Soc.*, 1956, **78**, 3557–3561.

[26] S. Berger, S. Braun and H.-O. Kalinowski, *^{31}P-NMR-Spektroskopie*, Georg Thieme Verlag, Stuttgart (Germany), 1993, vol. 3.

[27] G. M. Blackburn, J. S. Cohen and I. Weatherall, *Tetrahedron*, 1971, **27**, 2903–2912.

[28] G. M. Blackburn, J. S. Cohen and L. Todd, *Tetrahedron Lett.*, 1964, 2873.

[29] I. C. on Molecular Structure and Spectroscopy, *Pure Appl. Chem.*, 1972, **29**, 627–628.

[30] I. C. on Molecular Structure and Spectroscopy, *Pure Appl. Chem.*, 1976, **45**, 217–219.

[31] R. K. Harris, E. D. Becker, S. M. Cabral de Menezes, R. Goodfellow and P. Granger, *Solid State NMR*, 2002, **22**, 458–483.

[32] R. K. Harris, E. Becker, S. M. Cabral de Menezes, P. Granger, R. E. Hoffmann and K. W. Zilm, *Pure Appl. Chem.*, 2008, **80**, 59–84.

[33] C. van Wüllen, *Phys. Chem. Chem. Phys.*, 2000, **2**, 2137–2144.

[34] D. B. Chesnut and E. F. C. Byrd, *Heteroat. Chem.*, 1996, **7**, 307.

[35] D. B. Chesnut and B. E. Rusiloski, *Chem. Phys.*, 1991, **157**, 105–110.

[36] W. Kutzelnigg, U. Fleischer and M. Schindler, *The IGLO-Method: Ab-initio Calculation and Interpretation of NMR Chemical Shifts and Magnetic Susceptibilities*, in *NMR – Basic Principles and Progress*, ed. P. Diehl, E. Fluck, H. Günther, R. Kosfeld and J. Seelig, Springer, 1991, vol. 23, pp. 165–262.

[37] C. Adamo and V. Barone, *J. Chem. Phys.*, 1998, **108**, 664–675.

[38] G. Jeschke, W. Hoffbauer and M. Jansen, *Chem. Eur. J.*, 1998, **4**, 1755–1761.

[39] M. Jansen and B. Lüer, *Z. Kristallogr.*, 1986, **177**, 149–151.

[40] M. L. Walker, D. E. Peckenpaugh and J. L. Mills, *Inorg. Chem.*, 1979, **18**, 2792–2796.

[41] M. Jansen and S. Strojek, *Z. Naturforsch.*, 1997, **B52**, 906–910.

[42] W. Hoffbauer, S. Wefing, G. Klösters, F. Frick and M. Jansen, *Solid State Nucl. Magn. Reson.*, 1999, **14**, 211–.

[43] M. H. Möbs and M. Jansen, *Z. Anorg. Allg. Chem.*, 1984, **514**, 39–48.

[44] U. Fleischer, F. Frick, A. R. Grimmer, W. Hoffbauer, M. Jansen and W. Kutzelnigg, *Z. Anorg. Allg. Chem.*, 1995, **621**, 2012–2020.

[45] M. Jansen and M. Moebs, *Inorg. Chem.*, 1984, **23**, 4486–4488.

[46] A. C. Chapman, J. Homer, D. J. Mowthorpe and R. T. Jones, *J. Chem. Soc. Chem. Commun.*, 1965, 121–122.

[47] B. Beagley, D. W. J. Cruickshank, T. G. Hewitt and A. Haaland, *Trans. Faraday Soc.*, 1967, **63**, 836–845.

[48] D. G. Gorenstein, *Progr. NMR Spectrosc.*, 1983, **16**, 1–98.

[49] D. R. Lide, *CRC Handbook of Chemistry and Physics, CDROM Version*, CRC Press, 2003.

[50] K. Moedritzer, L. Maier and L. C. D. Groenweghe, *J. Chem. Eng. Data*, 1962, **7**, 307–310.

[51] L. Maier and R. Schmutzler, *J. Chem. Soc. Chem. Commun.*, 1969, **D**, 961–962.

[52] W. Althoff, M. Fild, H.-P. Rieck and R. Schmutzler, *Chem. Ber.*, 1978, **111**, 1845–1856.

[53] H. Oberhammer, *J. Mol. Struct.*, 1979, **53**, 139.

[54] V. A. Naumov, V. N. Semashko, A. P. Zav’yalov, R. A. Cherkasov and L. N. Grishina, *J. Struct. Chem. (Engl. Transl.)*, 1973, **14**, 739–742.

[55] P. Rovnaník, Z. Žák and M. Černík, *Z. Anorg. Allg. Chem.*, 2006, **632**, 1356–1362.

[56] H. S. Gutowski and D. W. McCall, *J. Chem. Phys.*, 1954, **22**, 162.

[57] M. Well, W. Albers, A. Fischer, P. G. Jones and R. Schmutzler, *Chem. Ber.*, 1992, **125**, 801–808.

[58] M. J. Frisch, G. W. Trucks, H. B. Schlegel, G. E. Scuseria, M. A. Robb, J. R. Cheeseman, J. A. Montgomery, Jr., T. Vreven, K. N. Kudin, J. C. Burant, J. M. Millam, S. S. Iyengar, J. Tomasi, V. Barone, B. Mennucci, M. Cossi, G. Scalmani, N. Rega, G. A. Petersson, H. Nakatsuji, M. Hada, M. Ehara, K. Toyota, R. Fukuda, J. Hasegawa, M. Ishida, T. Nakajima, Y. Honda, O. Kitao, H. Nakai, M. Klene, X. Li, J. E. Knox, H. P. Hratchian, J. B. Cross, V. Bakken, C. Adamo, J. Jaramillo, R. Gomperts, R. E. Stratmann, O. Yazyev, A. J. Austin, R. Cammi, C. Pomelli, J. W. Ochterski, P. Y. Ayala, K. Morokuma, G. A. Voth, P. Salvador, J. J. Dannenberg, V. G. Zakrzewski, S. Dapprich, A. D. Daniels, M. C. Strain, O. Farkas, D. K. Malick, A. D. Rabuck, K. Raghavachari, J. B. Foresman, J. V. Ortiz, Q. Cui, A. G. Baboul, S. Clifford, J. Cioslowski, B. B. Stefanov, G. Liu, A. Liashenko, P. Piskorz, I. Komaromi, R. L. Martin, D. J. Fox, T. Keith, M. A. Al-Laham, C. Y. Peng, A. Nanayakkara, M. Challacombe, P. M. W. Gill, B. Johnson, W. Chen, M. W. Wong, C. Gonzalez and J. A. Pople, *Gaussian 03, Revision D.01*, Gaussian, Inc., Wallingford, CT, 2004.

[59] M. Kaupp, in *Relativistic Electronic Structure Theory, Part 2: Applications*, ed. P. Schwerdtfeger, Elsevier, 2004, ch. 9, pp. 552–597.

[60] U. Haeberlen, *High Resolution NMR in Solids*, Academic Press, New York, 1976.

[61] C. Angeli, K. L. Bak, V. Bakken, O. Christiansen, R. Cimiraglia, S. Coriani, P. Dahle, E. K. Dalskov, T. Enevoldsen, B. Fernandez, C. Hättig, K. Hald, A. Halkier, H. Heiberg, T. Helgaker, H. Hettema, H. J. A. Jensen, D. Jonsson, P. Jørgensen, S. Kirpekar, W. Klopper, R. Kobayashi, H. Koch, A. Ligabue, O. B. Lutnæs, K. V. Mikkelsen, P. Norman, J. Olsen, M. J. Packer, T. B. Pedersen, Z. Rinkevicius, E. Rudberg, T. A. Ruden, K. Ruud, P. Sałek, A. S. de Meras, T. Saue, S. P. A. Sauer, B. Schimmelpfennig, K. O. Sylvester-Hvid, P. R. Taylor, O. Vahtras, D. J. Wilson and gren, *DALTON, a molecular electronic structure program, Release 2.0 (2005)*, http://www.kjemi.uio.no/software/dalton/dalton.html.

[62] E. J. Baerends, J. Autschbach, A. Bérces, F. M. Bickelhaupt, C. Bo, P. M. Boerrigter, L. Cavallo, D. P. Chong, L. Deng, R. M. Dickson, D. E. Ellis, M. van Faassen, L. Fan, T. H. Fischer, C. Fonseca Guerra, S. J. A. van Gisbergen, J. A. Groeneveld, O. V. Gritsenko, M. Grüning, F. E. Harris, P. van den Hoek, C. R. Jacob, H. Jacobsen, L. Jensen, G. van Kessel, F. Kootstra, E. van Lenthe, D. A. McCormack, A. Michalak, J. Neugebauer, V. P. Nicu, V. P. Osinga, S. Patchkovskii, P. H. T. Philipsen, D. Post, C. C. Pye, W. Ravenek, P. Ros, P. R. T. Schipper, G. Schreckenbach, J. G. Snijders, M. Solà, M. Swart, D. Swerhone, G. te Velde, P. Vernooijs, L. Versluis, L. Visscher, O. Visser, F. Wang, T. A. Wesolowski,

E. M. van Wezenbeek, G. Wiesenekker, S. K. Wolff, T. K. Woo, A. L. Yakovlev and T. Ziegler, *ADF2007.01*, SCM, Theoretical Chemistry, Vrije Universiteit, Amsterdam (Netherlands), 2008.

[63] J. F. Stanton, J. Gauss, J. D. Watts, P. G. Szalay, R. J. Bartlett and with contributions from A. A. Auer, D. B. Bernholdt, O. Christiansen, M. E. Harding, M. Heckert, O. Heun, C. Huber, D. Jonsson, J. Jusélius, W.J. Lauderdale, T. Metzroth, C. Michauk, D. P. O’Neill, D. R. Price, K. Ruud, F. Schiffmann, M. E. Varner, J. Vázquez and the integral packages MOLECULE (J. Almlöf and P. R. Taylor), PROPS (P. R. Taylor), and ABACUS (T. Helgaker, H.J. Aa. Jensen, P. Jørgensen, and J. Olsen), *Aces II, Mainz-Austin-Budapest version*, http://www.aces2.de, 2008.